npj Computational Materials

www.nature.com/npjcompumats

ARTICLE OPEN

Check for updates

Machine learning assisted design of γ′-strengthened Co-base superalloys with multi-performance optimization

Pei Liu[1,2], Haiyou Huang[1,2]✉, Stoichko Antonov[1,3], Cheng Wen[1,2], Dezhen Xue[4], Houwen Chen[5], Longfei Li[1,3], Qiang Feng[1,3], Toshihiro Omori[6] and Yanjing Su[1,2]✉

Designing a material with multiple desired properties is a great challenge, especially in a complex material system. Here, we propose a material design strategy to simultaneously optimize multiple targeted properties of multi-component Co-base superalloys via machine learning. The microstructural stability, γ′ solvus temperature, γ′ volume fraction, density, processing window, freezing range, and oxidation resistance were simultaneously optimized. A series of novel Co-base superalloys were successfully selected and experimentally synthesized from >210,000 candidates. The best performer, Co-36Ni-12Al-2Ti-4Ta-1W-2Cr, possesses the highest γ′ solvus temperature of 1266.5 °C without the precipitation of any deleterious phases, a γ′ volume fraction of 74.5% after aging for 1000 h at 1000 °C, a density of 8.68 g cm^{-3} and good high-temperature oxidation resistance at 1000 °C due to the formation of a protective alumina layer. Our approach paves a new way to rapidly design multi-component materials with desired multi-performance functionality.

npj Computational Materials (2020)6:62 ; https://doi.org/10.1038/s41524-020-0334-5

INTRODUCTION

As the key materials of the twenty-first century, aerospace alloys are of great economic value and developmental potential. Among them, superalloys are considered the most state-of-the-art, and are used to manufacture aeroengine and industrial gas turbine hot-end parts[1]. To safely operate in the harsh service environment, various properties, such as the temperature capability, density, high-temperature strength, as well as satisfactory resistance to hot-corrosion and oxidation under severe service conditions are highly desired[2,3]. Great efforts have been put forth to balance different alloying elements such as Al, Ti, Fe, Cr, Nb, Mo, W, and Ta in order to promote precipitation of stable γ′-Ni_3(Al, Ti), or a combination of γ′ and γ″-Ni_3Nb, meanwhile optimizing different aspects of the material performance[4]. However, these alloys are reaching their temperature capability limits, and novel design ideas are required to further improve engine performance and efficiency.

In 2006, Sato et al.[5] reported coherent, ordered $L1_2$ precipitate (γ′) strengthening in the Co-Al-W system, which has sparked interest in searching for novel γ′-strengthened Co-base superalloys with good performance to satisfy the aircraft and turbine application requirements and replace Ni-base superalloys. In the pursuit of higher temperature capability, many researchers have attempted to design γ′-strengthened Co-base superalloys with a higher γ′ solvus temperature. For example, Xue et al.[6] reported a quinary γ′-strengthened Co-base superalloy, Co-7Al-8W-4Ti-1Ta, which has a γ′ solvus temperature of 1131 °C and maintains stable γ′ precipitates after aging at 1050 °C for 1000 h. Furthermore, Lass et al.[7] reported the Co-30Ni-9Al-7W-4Ti-2Ta-0.1B alloy, which possesses an even higher γ′ solvus temperature, 1218 °C, and is devoid of any detrimental phase precipitation in the 900 °C to 1200 °C temperature range. However, lower density and improved oxidation resistance still remain as a major hurdle for these alloys, especially for long-term and higher temperature applications. As these various properties often compete, improving one is often at the expense of the other, and further improvement and optimization is needed[8].

One of the largest obstacles to the design of superalloys is the complexity from its multiple components, each of which is added with aim of improving a particular property. The design task is even more difficult when the goal is to optimize multiple properties simultaneously[2]. The traditional experimental alloy design approach to search for novel advanced superalloys through "trial and error" or intuition is thus inefficient[1]. Although novel design ideas such as diffusion multiples[9] and high-throughput thermodynamic calculations[7] have been introduced, they are still not efficient enough to solve such a complicated problem. What is needed is a high-efficiency method that enables discovery of superior multi-component superalloys with satisfactory multi-performance in an efficient and accelerated manner.

Statistical inference and machine-learning (ML) algorithms have been recently applied to discover advanced materials[10–15], and can adaptively guide the synthesis and characterization to select and optimize materials with desired properties. In the present study, utilizing data from both thermodynamic calculations and experiments, we combined ML with a global optimization algorithm to search for an optimized composition of a γ′-strengthened Co-base superalloy with desired multi-property performance. Considering the efficient balance of the ambiguous interaction among various elements and mutual inhibition between different properties, a design strategy of sequential filters composed of domain knowledge-driven empirical determination and ML models for different properties is employed to screen candidates, and an efficient global optimization (EGO) algorithm is then

[1]Beijing Advanced Innovation Center for Materials Genome Engineering, University of Science and Technology Beijing, 100083 Beijing, China. [2]Corrosion and Protection Center, University of Science and Technology Beijing, 100083 Beijing, China. [3]State Key Laboratory of Advanced Metals and Materials, University of Science and Technology Beijing, 100083 Beijing, China. [4]State Key Laboratory for Mechanical Behavior of Materials, Xi'an Jiaotong University, 710049 Xi'an, China. [5]College of Materials Science and Engineering, Chongqing University, 400044 Chongqing, China. [6]Department of Materials Science, Graduate School of Engineering, Tohoku University, Sendai 980-8579, Japan. ✉email: huanghy@mater.ustb.edu.cn; yjsu@ustb.edu.cn

Published in partnership with the Shanghai Institute of Ceramics of the Chinese Academy of Sciences

npj nature partner journals

utilized to recommend potential target materials. The best alloy obtained from only three rounds of new experiments, Co-36Ni-12Al-2Ti-4Ta-1W-2Cr, outperforms many reported Co-base alloys in terms of the overall performance of this study. Our approach is general and applicable to various materials design problems aimed at optimizing multiple properties.

RESULTS

Material design

Among all of the properties of the γ′-strengthened Co-base superalloys, the γ′ solvus temperature is of the greatest importance, as it determines the upper temperature capability limit. Therefore, in order to develop advanced single crystal materials, a high γ′ solvus temperature (>1250 °C) is needed. Additionally, the processing window ($\Delta T_p = T_{solidus} - T_{\gamma'\text{-solvus}} \geq 40$ °C), freezing range ($\Delta T_f = T_{liquidus} - T_{solidus} \leq 60$ °C), density ($\rho \leq 8.7$ g cm^{-3}), and microstructural stability were also considered simultaneously as targeted properties to be optimized by ML. Owing to insufficient experimental-data in thermodynamic databases, the oxidation resistance (giving priority to obtain protective alumina layer) and γ′ volume fraction ($V_{\gamma'} \geq 60\%$) are considered empirically based on results of previous studies[16–20], i.e., by setting thresholds for associated elements.

The $Co_aAl_bW_cNi_dTi_eTa_fCr_g$ family was chosen as the system to be optimized. The potential composition space was defined as follows (the concentration of elements are in atomic percent): $30\% \leq a \leq 100\%$, $10\% \leq b \leq 15\%$, $1\% \leq c \leq 8\%$, $20\% \leq d \leq 50\%$, $1\% \leq e \leq 8\%$, $1\% \leq f \leq 4\%$, $2\% \leq g \leq 10\%$, and each alloy in this space is constrained by $a > d$ and $a + b + c + d + e + f + g = 100\%$. The beneficial effect of Al and Cr on the environmental resistance of superalloys is most potent among the selected elements[16]. In order to meet the requirements for adequate oxidation resistance, and based on the study of Stewart et al.[17], the lower and upper limits of the Al content in the composition space were set as 10 at.% and 15 at.%, respectively. Despite the negative effect of Cr on the γ′ solvus temperature, Cr still plays an irreplaceable role in the oxidation resistance of the alloy at elevated temperatures by stabilizing the Al_2O_3 oxide[18]. Therefore, we set the Cr content to be no <2 at.% and no >10 at.%. To ensure an appropriate γ′ volume fraction[19,20], while ensuring lower density, the lower limits of the other γ′-forming elements—W, Ta, and Ti—were all set as 1%. In this composition space, we calculated the number of candidates that satisfy these two constraints exhaustively with a computer program. A composition variation step of 1 at.% for each element gives a total of 210792 unknown compositions to be evaluated.

Machine-learning strategy

The material design strategy for multi-performance optimization in Co-base superalloys is shown in Fig. 1, and includes three parts: sequential filters, EGO, experimental verification and feedback. The sequential filters comprise of domain knowledge-driven empirical determination (we define the rational composition space by the summarized experiences from predecessors to control the properties of compositions without available data), computational-data driven phase classification and experimental-data driven performance regression. Prior to any property optimization, the first consideration is the high-temperature and long-term microstructural stability of the alloys, as the precipitation of β, μ, and other related topologically close-packed (TCP) phases poses negative effects on the mechanical properties, and should be avoided as much as possible[21]. Thus, a ML classification model can be built and applied to obtain a potential composition space, which contains only γ and γ′ two-phase microstructures. However, as there is insufficient experimental-data, and the thermodynamic database could be a better choice. Li et al.[22] used the thermodynamic database-Pandat™ to design multi-component Co-base superalloys without deleterious phases after aging at 1100 °C for 1000 h. Zhuang et al.[23] also designed a novel γ′-strengthened Co-base wrought superalloy with desired

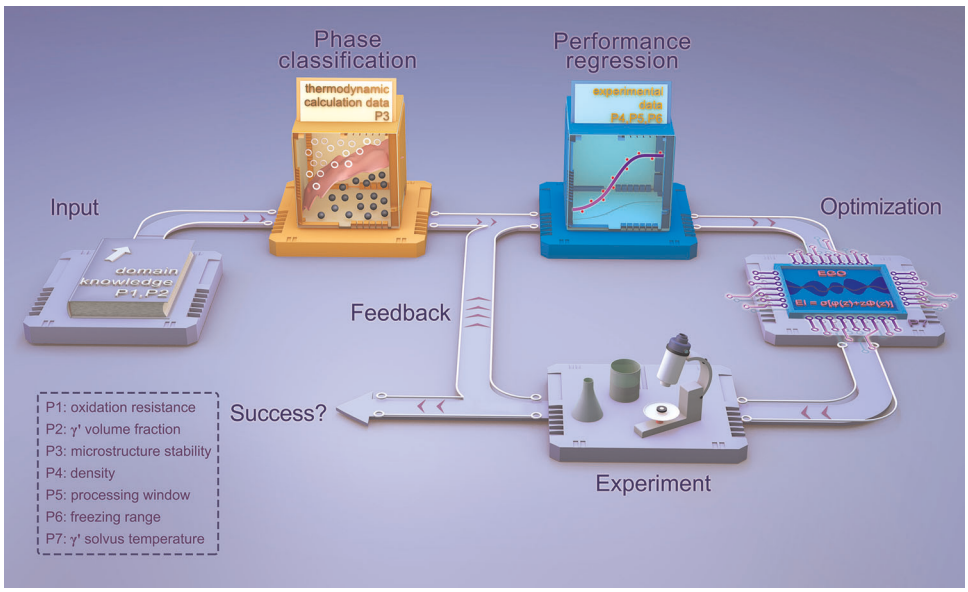

Fig. 1 A material design strategy for multi-performance optimization in multi-component Co-base superalloys by machine learning. Based on the potential composition space determined by the domain knowledge, the thermodynamic calculation data are used for the phase classification model, and the experimental-data for density, γ′ solvus temperature, solidus and liquidus are used for the corresponding performance regression models. According to the sequential filters, these predictions are applied to screen the potential composition space for optimization. Machine learning with the optimization algorithm is used to guide this workflow and to find promising candidates with high γ′ solvus temperature. Four predicted alloys with the largest expected improvement (EI) values are selected to experimentally synthesize and characterize. The experimental results (γ′ solvus temperature, solidus, liquidus and density) of successfully processed new alloys were fed back to the regression models to refine them, and the optimization was iterated again until to find the alloys with targeted properties.

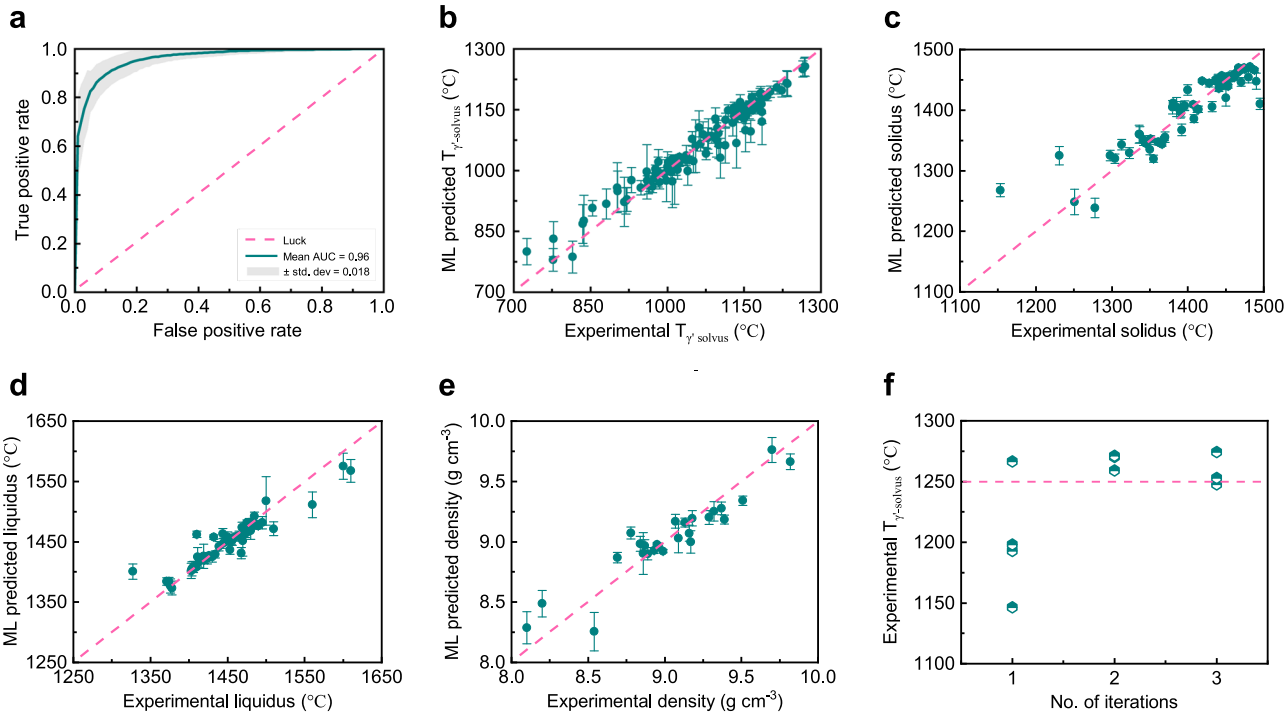

Fig. 2 Machine-learning models and iteration results. a The ROC curve is used to evaluate the merit of classification models. The values of abscissa and ordinate axes are false-positive rate and true positive rate, respectively. The gray area represents the standard deviation of 100 ROC curves, and the pink dashed line represents a random classification such as coin tossing. **b**–**e** The performance of best regression model on the testing dataset for the γ′ solvus temperature, solidus, liquidus and density, respectively. Experimental (axis of abscissa) and ML predicted (axis of ordinate) values represent each property in the respective original dataset. The error bars are the standard deviation from the predictions of 1000 regression models corresponding to each property, and the pink dotted line represents the same predictions from ML models as the experimental values. **f** The experimental values as a function of iteration number. We iterate our experiment group for a total of three times, and a flat tendency emerges among the highest values. The pink dashed line represents the target value.

microstructure by CALPHAD method. They mean good reliability of this thermodynamic database in controlling phase equilibrium. Therefore, we utilized thermodynamic computations to generate a training dataset for the ML classification model. Specifically, we used Pandat™ with the Co-base thermodynamic library PanCo2018 to produce 1000 phase fraction plots to be used as data. Within the desired temperature window between 900 °C and 1300 °C, there were 500 compositions corresponding to a γ/γ′ two-phase microstructures, which are labeled as "0", and another 500 compositions exhibiting the precipitation of detrimental phases, which are labeled as "1". In order to improve the adaptability and robustness of the phase classification model, the chemical compositions together with the composition-weighted mean value of three physical parameters (valence electron number, first energy ionization and effective charge nuclear (Clementi)) were used as the material descriptors. The four different classification algorithms were compared to obtain the optimal phase classification model. Receiver operating characteristic (ROC) curves revealing the classification capability are employed to select the optimal model. A large area under the ROC curve (AUC) ensures a better classifier. The mean value of 100 AUC for the gradient tree boosting (GTB) classification model is 0.96, as shown in Fig. 2a. The value is larger than the other models, indicating that a high accuracy and good classification performance (details of AUC for the four classification models are shown in the Supplementary Table 1). Therefore, the GTB classification model was chosen as the classifier for each alloy in the potential composition space to predict whether it possesses only a γ and γ′ two-phase microstructure.

Regression models were built to predict the γ′ solvus temperature, solidus, liquidus and density based on an experimental dataset assembled from the literature[6,7,16,18–22,24–54] and our own experiments. The number of data points in the original dataset for the γ′ solvus temperature, solidus, liquidus, and density was 134, 94, 68 and 31, respectively. We built six different regression models, and used the chemical compositions as the descriptors. The mean-squared error (MSE) was used to evaluate the quality of the regression models, and the model with the minimal MSE was selected. Among the six typical models, as shown in Fig. 2(b–e), the best model corresponding to the γ′ solvus temperature, solidus, liquidus and density were the GTB, random forest (RF), GTB and GTB, respectively (details of MSE values for each regression model are shown in the Supplementary Table 2). Then, the sequential filters were fully assembled by domain knowledge-driven empirical determination, computational-data driven phase classification and experimental-data driven performance regression for the optimization of multi-property performance. Owing to this rigorous screening by sequential filters, the composition space originally consisting of 210,792 unknown alloys was reduced to <6000 compositions.

In order to avoid the prediction result of the regression model trained by small data into local extremum, we adopt a global optimization algorithm EGO[55] to search for desired alloys with high γ′ solvus temperature (the main targeted property). We utilized bootstrap sampling to attain the prediction value and the associated uncertainty. In detail, we generate a bootstrap training set by resampling the data from the original training data with replacement. We trained 1000 models based on 1000 bootstrapped datasets to obtain 1000 predictions of γ′ solvus temperature for each alloy in the unexplored composition space. The mean predicted value and standard deviation can be estimated from the 1000 predictions to obtain the expected improvement (EI) for each alloy (details are presented in "Methods"). In order to select a batch of alloys as the experimental group, the alloy with the largest EI value is selected to put into the

Table 1. The alloys predicted from iterative workflow by machine learning and their experimental properties.

Alloy no.	Composition	Detrimental phase	$V_{\gamma'}$ (%)	$T_{\gamma'\text{-solvus}}$ (°C)	$T_{solidus}$ (°C)	$T_{liquidus}$ (°C)	Processing window (°C)	Freezing range (°C)	ρ (g cm^{-3})	Mass gain (mg cm^{-2})
1–1	Co-20Ni-10Al-5Ti-4Ta-1W-7Cr	1	–	1193.0	1242.1	1273.4	49.1	31.3	8.61	0.29
1–2	Co-36Ni-12Al-2Ti-4Ta-1W-2Cr	0	74.5	1266.5	1315.6	1362.4	49.1	46.8	8.68	1.99
1–3	Co-21Ni-10Al-5Ti-4Ta-1W-7Cr	1	–	1198.2	1242.2	1276.4	44.0	34.2	8.61	0.31
1–4	Co-25Ni-12Al-2Ti-4Ta-1W-10Cr	1	–	1146.3	1274.0	1311.4	127.7	37.4	8.55	0.36
2–1	Co-38Ni-12Al-3Ti-4Ta-2W-2Cr	Failed to process								
2–2	Co-36Ni-12Al-3Ti-4Ta-1W-2Cr	1	–	1259.1	1295.2	1344.2	36.1	49.0	8.61	2.51
2–3	Co-36Ni-11Al-3Ti-4Ta-1W-2Cr	1	–	1270.2	1300.7	1352.0	30.5	51.3	8.68	3.38
2–4	Co-36Ni-13Al-2Ti-4Ta-1W-2Cr	1	–	1271.3	1305.8	1355.1	34.5	49.3	8.59	2.26
3–1	Co-38Ni-13Al-2Ti-4Ta-1W-2Cr	1	–	1274.4	1305.6	1352.5	31.2	46.9	8.61	1.61
3–2	Co-38Ni-10Al-4Ti-4Ta-3W-2Cr	Failed to process								
3–3	Co-36Ni-11Al-2Ti-4Ta-2W-2Cr	0	76.8	1247.6	1319.6	1364.7	72.0	45.1	8.87	4.32
3–4	Co-36Ni-13Al-1Ti-4Ta-1W-2Cr	0	79.9	1252.8	1323.0	1365.3	70.2	42.3	8.63	3.39

Apart from the two alloys that could not be processed (homogenized), the experiment and characterization results of the other ten alloys are provided. The nominal composition (at.%) is used to represent these alloys, which is nearly consistent with the measured composition detected by EDS in FE-SEM (measured compositions are shown in Supplementary Table 3). The criterion for judging the existence of detrimental phase is based on the microstructure of the alloy aged at 1000 °C for 1000 h, and a label of "1" represents the appearance of detrimental phases and a label of "0" means an absence. The γ′ volume fraction is obtained from the mean value of five different microstructure images. The $T_{\gamma'\text{-solvus}}$, $T_{solidus}$, $T_{liquidus}$ are obtained by DSC heating curves. The density is measured based on Archimedes displacement principle. The mass gain of each alloy is acquired after isothermal oxidation at 1000 °C for 100 h.

training data with its predicted value, then the model is refined and another alloy with the largest EI value is chosen in the next iteration. We repeat this procedure until we obtain a recommendation of four candidate alloys as the experimental group. These alloys are synthesized and characterized, and the results are fed back to augment the training dataset. The loop is executed iteratively until the alloys with good targeted performance are discovered. As shown in Fig. 2f, we iterate our experimental group for a total of three times until the newly made alloy's γ′ solvus temperature reaches >1250 °C, and the γ′ solvus temperature of the experimental alloys no longer increases significantly.

Multi-performance optimization

The synthesized alloys from the iterative loop are given in Table 1 (more experimental results are collected in the Supplementary information). We conducted a total of three rounds of new experiments, fabricating four alloys each round (as for the abbreviation of each alloy, the first number gives the iteration round, and the second represents alloy with the highest EI value in the respective computational loop, e.g., Alloy 1–2 is the alloy with the highest EI value in the second computational loop of the first round). Based on the aim of optimizing multiple properties in this study, Alloy 1–2 is the preferred composition with the highest γ′ solvus temperature that simultaneously meets the demands of all targeted properties. The microstructure of Alloy 1–2 is shown in Fig. 3a. The γ′ volume fraction of the alloy is 74.5%, and it doesn't exhibit any detrimental phase after aging at 1000 °C for 1000 h. The differential scanning calorimetry (DSC) heating curve of Alloy 1–2 is shown in Fig. 3b. Alloy 1–2 has a γ′ solvus temperature of 1266.5 °C, and the processing window and freezing range are 49.1 °C and 46.8 °C, respectively, which are suitable for practical manufacturing. The density of Alloy 1–2 is 8.68 g cm^{-3}, which is less than the threshold set by the ML model and also less than the density of some advanced Ni-base single crystal superalloys (e.g., René N6 and CMSX-10)[56]. This is beneficial for reducing the weight of aero-engines and improving the overall aircraft efficiency. Owing to the lack of high-quality experimental-data with a unified standard, a prior knowledge approach was used to ensure good high-temperature oxidation resistance of the superalloy, by controlling the content of Al and Cr in the composition space based on the valuable experiences from previous studies[16–18]. The representative microstructure of the oxides and the oxidation mass gain curves of three selected alloys (Alloy 1–2, Alloy 3-3, and Alloy 3–4) after oxidation at 1000 °C are shown in Fig. 3(c–d). The oxidation mass gain of Alloy 1–2 is around 1.99 mg cm^{-2} which is the lowest in the three selected alloys. A protective layer of alumina formed after isothermal oxidation, representatively shown in Fig. 3d for Alloy 1–2.

Only three alloys did not precipitate detrimental phases after aging at 1000 °C for 1000 h, whereas for the other recommended alloys, all of the properties except the microstructural stability are acceptable. Based on the experimental results, the higher the γ′ solvus temperature, the higher the needed alloying content to achieve it, and hence the greater the propensity for precipitation of detrimental phases. Therefore, the predicted alloy compositions are likely located at the phase classification boundary. As it is not trivial to make an accurate phase classification model in a multi-component system using only thermodynamic calculation data where phase boundaries are often not known to a high degree of accuracy, most synthesized alloys precipitated deleterious phases. This can be alleviated with the use of more accurate thermodynamic data, or through improved fabrication techniques utilizing vacuum induction melting and electro-slag remelting for tight compositional control and reduction of tramp elements.

We used just three rounds of experiments to find new desired alloys that satisfy our design targets under the ML guidance, and the γ′ solvus temperatures of these alloys are higher when

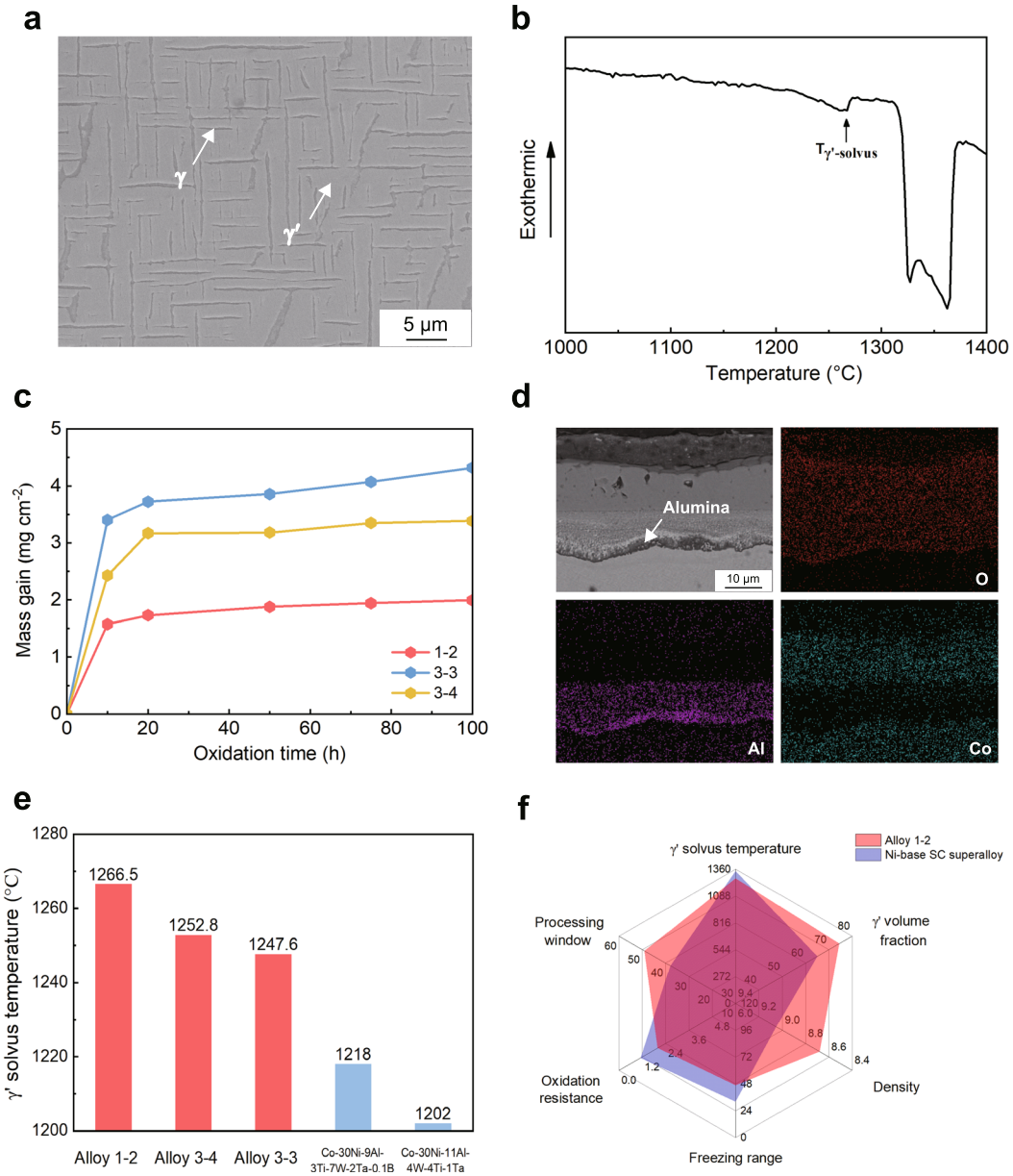

Fig. 3 The multiple properties optimized for Alloy 1–2. a The typical microstructure consists of γ/γ′ phases without detrimental phase after aging at 1000 °C for 1000 h. **b** The DSC heating curve of Alloy 1–2. **c** Mass gain per surface area during isothermal oxidation test of the three TCP-free alloys 1–2, 3-3, and 3–4 performed at 1000 °C. **d** The microstructure and distribution of selected elements for the oxide scale of Alloy 1–2 oxidized at 1000 °C for 10 h, consisting of a protective alumina layer formed on the surface of the alloy. **e** The three of the ten synthesized alloys that possess the highest $T_{\gamma'\text{-solvus}}$ and are free of any detrimental phases after aging for 1000 h at or above 1000 °C. **f** The radar charts of some representative properties (γ′ solvus temperature (°C), γ′ volume fraction (%), density (g cm^{-3}), freezing range (°C), oxidation resistance (mass gain (mg cm^{-2})), and processing window (°C)) of Alloy 1–2 and advanced Ni-base single crystal superalloy[56,58–60], showing the balance of multiple properties achieved for Alloy 1–2.

compared with previously reported alloys[7,22], without exhibiting detrimental phases after high-temperature long-term aging, as shown in Fig. 3e. Compared with oxidation-resistant alloy SB-CoNi-10 that has a low density (8.65 g cm^{-3}) and a high γ′ solvus temperature (1196 °C)[57], the γ′ solvus temperature of Alloy 1–2 is about 70 °C higher than that of alloy SB-CoNi-10. The different properties optimized in this study (using Alloy 1–2 as an example) are comparable to advanced Ni-base single crystal superalloys[56,58–60], such as CMSX-10, as shown in Fig. 3f. Such rapid optimization and ability to achieve well-balanced properties is a breakthrough for this class of superalloys, although a small amount of the γ′ solvus temperature, freezing range and oxidation resistance were sacrificed, compared to CMSX-10, in order to improve the other targeted properties. Therefore, the best performer, Co-36Ni-12Al-2Ti-4Ta-1W-2Cr alloy, warrants further research whether it meets other unstudied properties requirements to use as single crystal material, and to serve as a base for further optimization and development.

DISCUSSION

In order to further understand the elemental distribution to the γ and γ′ phases of the experimental alloys, elemental mapping was performed with high-angle annular dark field (HAADF) scanning transmission electron microscope (STEM) nanoprobe and accurate phase compositions were measured using atom probe

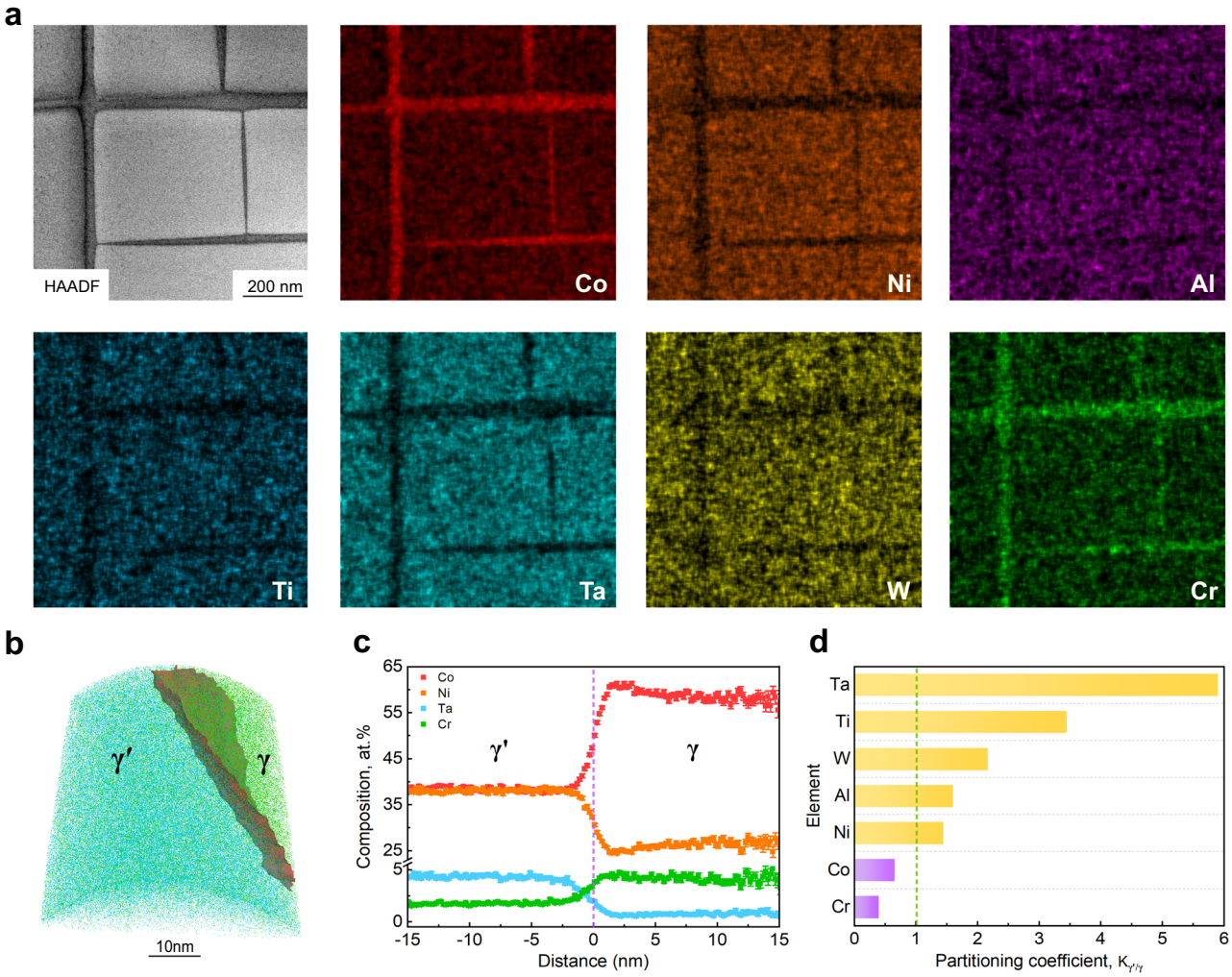

Fig. 4 The microstructure characterization of Alloy 1–2 after annealing at 1000 °C for 50 h. a STEM HAADF image and elemental mapping for the γ/γ′ precipitate using an STEM nanoprobe. **b** APT three-dimensional reconstruction. **c** A proximity histogram concentration profile of major elements across the γ/γ′ interface based from the APT sample reconstruction. **d** Partitioning coefficients of solute elements. The yellow bars represent the elements that preferentially distribute in the γ′ phase ($K^X_{\gamma'/\gamma} > 1$), and the purple bars represent the elements that partition strongly to the γ phase ($K^X_{\gamma'/\gamma} < 1$).

tomography (APT) for Alloy 1–2. From this data, the partitioning coefficients $K^X_{\gamma'/\gamma} = C^X_{\gamma'}/C^X_{\gamma}$ of each element, where $C^X_{\gamma'}$ and C^X_{γ} are equilibrium concentrations of element *X* in the γ′ and γ phases, were calculated. As shown in Fig. 4a, distinct cuboidal γ′ precipitates are distributed in the γ phase matrix, and elements such as Ta, Ti, W, Al, and Ni preferentially partition to the γ′ phase, while elements such as Co and Cr partition strongly to the γ phase. Based on the quantitative APT results (Fig. 4(b–d)), the partitioning coefficient of Ta is the largest ($K^{Ta}_{\gamma'/\gamma} = 5.90$). Hence, it has the greatest positive effect on the stabilization of the γ′ phase as a γ′-forming element, and is also advantageous to increase the $T_{\gamma'\text{-solvus}}$. This is further supported by the Ta content of the alloy, which has reached the upper limit of our potential composition space during the optimization by the ML model. As a γ phase forming element, Cr mainly partitions to the γ phase, resulting in the smallest partitioning coefficient ($K^{Cr}_{\gamma'/\gamma} = 0.40$) among the elements, hence it is not favorable for improving the γ′ phase stability and $T_{\gamma'\text{-solvus}}$ of the alloy. Consequently, in agreement with the trends obtained by ML, the content of Cr in the alloy has reached the lower limit in the composition space. Compared to the partitioning coefficients reported by other studies in the existing literatures[61–63], the partitioning trend and extent of each element is consistent even though these elements contained in different Co-base alloys. Under the same aging conditions, the partitioning of each element is mainly affected by the chemical compositions and ambiguous interaction among various elements. These results of partitioning coefficients demonstrate the black-box ML models could detect the inner partitioning mechanism of each element, and provide the active guidance in the optimization of multiple properties and compositions. Comparing the Co and Ni contents in the two phases, Co is the major element of the γ matrix (59.4 at.%), followed by Ni (25.6 at.%), while their contents are nearly equal in the γ′ phase. A higher Ni content in the alloy expands the γ-γ′ two-phase field and increases the stability of the alloy[22,64], which is clearly captured by the ML approach. This also suggests that the future research direction is likely the design of Ni-rich Co-base superalloys (also known as CoNi-base superalloy) with desired multi-properties.

To summarize, a machine-learning framework was used to efficiently obtain optimized γ′-strengthened Co-base superalloys through three rounds of new experiments based on a multi-performance criterion. These alloys are comparable with some advanced Ni-base single crystal superalloys, and warrant further research for additional properties that were not involved in this

study (e.g., creep and fatigue) to determine whether they meet the requirements for industrial application. Benefiting from the use of sequential filters and EGO algorithm, multiple optimized properties are balanced efficiently, and the time and cost of material discovery are greatly reduced. Specifically, the introduction of sequential filters driven by domain knowledge and machine-learning models greatly narrows the vast composition space to be optimized, resulting in the best performer, Co-36Ni-12Al-2Ti-4Ta-1W-2Cr, obtained by only three rounds of new experiments assisted with EGO. Our research provides a fast and efficient machine-learning method to optimize multiple properties of superalloys, which also showcases a typical case study for utilizing machine learning in extremely complex material design problems. This material design strategy driven by machine learning is general and is not limited to the multi-performance optimization of superalloys but also applicable to other multi-component materials such as high-entropy alloys, superconductors, ceramics and perovskite-type materials, etc. It provides a new material design method for the research and development of advanced materials.

METHODS

Machine-learning models

The logistic regression, decision tree, AdaBoost and GTB classification algorithms were used to train these classification models, and the hyperparameters of each model were tuned by ten-fold cross-validation. The ROC curve is very effective in evaluating the performance of the binary classification model. The closer the curve is to the upper left corner, the higher the reliability of the classification model. The AUC value is the area under the ROC curve, and can be used to quantify the merit of the ROC curve. The closer the AUC value is to 1, the better the performance of the model. We utilized the method of hold-out to obtain a reliable AUC value, 90% of the original data were randomly chosen as training set to train the model and 10% of the data were used as a testing set to verify the predictive capability of the model. Thus, 100 models of four different algorithms were obtained. The mean value of 100 AUC values was taken as the metric to reflect the classification capability of the model. The method of hold-out was also used to train the performance regression models of solidus, liquidus and density. The 1000 models of the AdaBoost, decision tree, support vector machine with a kernel of radial basis function, k-nearest neighbors, RF and GTB regression algorithms were used to build the regression models based on the original dataset. The $\mathrm{MSE} = \sum_{i=1}^{n} (y_i - \hat{y}_i)$, (where (y_i) is the true value and $(\hat{y}_i)$ is the predicted value) was used to evaluate the predictive capability of different regression models, and the models with the minimal MSE (the mean MSE value of 1000 models) was selected for use.

Efficient global optimization

In the present study, we use a powerful optimization strategy called EGO, which can balance the exploitation and exploration by an adaptive iteration loop, shown in Fig. 1. Expected improvement (EI) is employed to select the next experimental candidate, such as an alloy with higher γ′ solvus temperature. Subsequent alloy synthesis and experiments allow an iterative improvement of the surrogate model by incorporating the measured results into the training dataset. The calculation of EI is given by $\mathrm{EI} = \sigma[\varphi(z) + z\Phi(z)]$, where $z = T_{\gamma'\text{-solvus}} - \mu^*)/\sigma$ and μ^* is the maximum γ′ solvus temperature in the original dataset, $\varphi(z)$ and $\Phi(z)$ are the standard normal density and cumulative distribution functions, respectively. It can be seen that the EI is not only related to the exploitation (model-predicted value u), but also to the exploration (uncertainty of prediction σ). Maximizing EI provides an optimization approach to balance these two extremes and help to navigate to the target alloy efficiently. This machine-learning procedure was implemented in Python using the publicly available library of Numpy/Scipy and scikit-learn (version 0.19.1).

Experimental process

Raw metals with purity higher than 99.95% were used, and the oxides and impurities on the surface of the raw metals were removed before processing the alloy. In order to ensure the homogeneity of the alloy composition and facilitate comparison, the alloy button ingots were prepared by vacuum arc melting, where each 30 g alloy was melted at least six times. The Archimedes displacement principle was applied to measure the density of each alloy five times and the mean value was taken. After ultrasonic cleaning, the as-cast ingot was sealed in quartz tube filled with high purity argon, and then subjected to solution heat treatment at 1200–1280 °C for 24 h followed by air cooling. All samples were cut and subsequently aged at 1000 °C for 50 h followed by water cooling. The γ′ solvus, solidus and liquidus temperatures were determined by DSC (NETZSCH STA 449C) with high purity Ar flow. The samples for DSC of size φ 3 mm × 1 mm were tested in a temperature range of 800–1400 °C at a heating rate of 5 °C min^{-1}. The line intercept method was used to measure the transformation temperatures based on the DSC heating curves. All samples were metallographically prepared using standard techniques, and etched for a few seconds using a solution of HNO_3: HCl: H_2O = 1: 1: 1. The microstructure was characterized with a Zeiss GeminiSEM 300 field-emission scanning electron microscope (FE-SEM) in secondary electron imaging mode, and equipped with energy-dispersive X-ray spectroscopy (EDS) detector, used to measure the alloy composition. The crucible used for isothermal oxidation was pre-fired at 1050 °C until the weight change of the crucible was $<2 \times 10^{-4}$ g, and then considered to be constant weight. Isothermal oxidation experiments were carried out at 1000 °C for 100 h. The weight of the sample and crucible was measured by an electronic analytical balance with sensitivity down to 10^{-5} g before and after oxidation. The oxidized samples Ni-plated to preserve the oxide layers. The oxides microstructure was characterized with the FE-SEM in backscattered electron imaging mode, and EDS was used to detect the element distribution of the oxides. Thin foil specimens for the TEM observation were prepared by ion-thinning. STEM observations and energy-dispersive X-ray spectrometry (EDS) analysis were performed in a Cs-corrected FEI Titan G2 60–300 ChemiSTEM, equipped with Super-X EDS detectors and operated at 300 kV. Specimens for APT analysis were then extracted and fabricated from select sites using a dual beam SEM/focused-ion-beam instrument via an in-situ lift-out protocol. A final cleaning procedure was carried out at 5 kV and 15 pA beam current to remove regions severely damaged by the high-energy (30 kV) Ga ion beam. The APT measurements were conducted using a LEAP™ 5000XR instrument (Cameca Instruments). Laser pulsing mode operation was applied at a pulse repetition rate of 125 kHz and a pulse energy of 40 pJ. The specimen's base temperature was kept at 30 K, and the target detection rate was set to five ions detected every 1000 pulses. Data analysis was performed using the software package IVAS™ 3.8.2. To further study the microstructural stability of the alloy, the experimental samples were subjected to long-term aging of 1000 h at 1000 °C, respectively. The γ′ volume fraction was obtained from the mean value of five different microstructure images by Image-Pro plus 6.0 software.

DATA AVAILABILITY

The data that support the findings of this study are available from the corresponding author upon reasonable request.

CODE AVAILABILITY

The codes that support the findings of this study are available from the corresponding author upon reasonable request.

Received: 4 October 2019; Accepted: 5 May 2020;
Published online: 25 May 2020

REFERENCES

1. Reed, R. C. *The Superalloys: Fundamentals and Applications* (Cambridge University Press, 2006).
2. Pollock, T. M. Alloy design for aircraft engines. *Nat. Mater.* **15**, 809–815 (2016).
3. Darolia, R. Development of strong, oxidation and corrosion resistant nickel-based superalloys: critical review of challenges, progress and prospects. *Int. Mater. Rev.* **64**, 355–380 (2019).
4. Pollock, T. M. & Tin, S. Nickel-based superalloys for advanced turbine engines: Chemistry, microstructure, and properties. *J. Propul. Power* **22**, 361–374 (2006).
5. Sato, J. et al. Cobalt-base high-temperature alloys. *Science* **312**, 90–91 (2006).
6. Xue, F., Zhou, H. J., Ding, X. F., Wang, M. L. & Feng, Q. Improved high temperature γ′ stability of Co-Al-W-base alloys containing Ti and Ta. *Mater. Lett.* **112**, 215–218 (2013).

7. Lass, E. A. Application of computational thermodynamics to the design of a Co-Ni-based γ′-strengthened superalloy. *Metall. Mater. Trans. A.* **48**, 2443–2459 (2017).
8. Suzuki, A., Inui, H. & Pollock, T. M. $L1_2$-strengthened cobalt-base superalloys. *Annu. Rev. Mater. Res.* **45**, 345–368 (2015).
9. Zhu, L. L. et al. Experimental investigation of phase equilibria in the Co-rich part of the Co-Al-X (X = W, Mo, Nb, Ni, Ta) ternary systems using diffusion multiples. *J. Alloy. Compd.* **691**, 110–118 (2017).
10. Raccuglia, P. et al. Machine-learning-assisted materials discovery using failed experiments. *Nature* **533**, 73–77 (2016).
11. Xue, D. et al. Accelerated search for materials with targeted properties by adaptive design. *Nat. Commun.* **7**, 11241 (2016).
12. Yuan, R. H. et al. Accelerated discovery of large electrostrains in $BaTiO_3$-based piezoelectrics using active learning. *Adv. Mater.* **30**, 1702884 (2018).
13. Wen, C. et al. Machine learning assisted design of high entropy alloys with desired property. *Acta Mater.* **170**, 109–117 (2019).
14. Wang, C., Fu, H., Jiang, L., Xue, D. & Xie, J. A property-oriented design strategy for high performance copper alloys via machine learning. *NPJ Comput. Mater.* **5**, 87 (2019).
15. Zhang, Y. et al. Phase prediction in high entropy alloys with a rational selection of materials descriptors and machine learning models. *Acta Mater.* **185**, 528–539 (2020).
16. Ismail, F. B. et al. Alloying effects on oxidation mechanisms in polycrystalline Co–Ni base superalloys. *Corros. Sci.* **116**, 44–52 (2017).
17. Stewart, C. A., Rhein, R. K., Suzuki, A., Pollock, T. M. & Levi, C. G. Oxide scale formation in novel γ-γ′ cobalt-based alloys. *Superalloys* **2016**, 991–999 (2016).
18. Klein, L., Shen, Y., Killian, M. S. & Virtanen, S. Effect of B and Cr on the high temperature oxidation behaviour of novel γ/γ′-strengthened Co-base superalloys. *Corros. Sci.* **53**, 2713–2720 (2011).
19. Murakumo, T., Kobayashi, T., Koizumi, Y. & Harada, H. Creep behaviour of Ni-base single-crystal superalloys with various γ′ volume fraction. *Acta Mater.* **52**, 3737–3744 (2004).
20. Ooshima, M., Tanaka, K., Okamoto, N. L., Kishida, K. & Inui, H. Effects of quaternary alloying elements on the γ′ solvus temperature of Co-Al-W based alloys with fcc/$L1_2$ two-phase microstructures. *J. Alloy. Compd.* **508**, 71–78 (2010).
21. Omori, T. et al. Partition behavior of alloying elements and phase transformation temperatures in Co-Al-W-base quaternary systems. *Intermetallics* **32**, 274–283 (2013).
22. Li, W., Li, L., Antonov, S. & Feng, Q. Effective design of a Co-Ni-Al-W-Ta-Ti alloy with high γ′ solvus temperature and microstructural stability using combined CALPHAD and experimental approaches. *Mater. Des.* **180**, 107912 (2019).
23. Zhuang, X., Lu, S., Li, L. & Feng, Q. Microstructures and properties of a novel γ′-strengthened multi-component CoNi-based wrought superalloy designed by CALPHAD method. *Mater. Sci. Eng. A.* **780**, 139218 (2020).
24. Dmitrieva, G., Vasilenko, V. & Melnik, I. Al-Co-W fusion diagram in the Co-CoAl-W part. *Chem. Met. Alloy.* **1**, 338–342 (2008).
25. Shinagawa, K. et al. Phase equilibria and microstructure on γ′ phase in Co-Ni-Al-W system. *Mater. Trans.* **49**, 1474–1479 (2008).
26. Suzuki, A. & Pollock, T. M. High-temperature strength and deformation of γ/γ′ two-phase Co-Al-W-base alloys. *Acta Mater.* **56**, 1288–1297 (2008).
27. Tanaka, K., Ooshima, M., Okamoto, N. L., Kishida, K. & Inui, H. Morphology change of γ′ precipitates in γ/γ′ two-phase microstructure in Co-based superalloys by higher-order alloying. *2011 MRS Spring Meeting*, 423–428 (2011).
28. Kobayashi, S., Tsukamoto, Y. & Takasugi, T. Phase equilibria in the Co-rich Co-Al-W-Ti quaternary system. *Intermetallics* **19**, 1908–1912 (2011).
29. Meher, S., Yan, H.-Y., Nag, S., Dye, D. & Banerjee, R. Solute partitioning and site preference in γ/γ′ cobalt-base alloys. *Scr. Mater.* **67**, 850–853 (2012).
30. Tanaka, K., Ooshima, M., Tsuno, N., Sato, A. & Inui, H. Creep deformation of single crystals of new Co–Al–W-based alloys with fcc/$L1_2$ two-phase microstructures. *Philos. Mag.* **92**, 4011–4027 (2012).
31. Omori, T. et al. Experimental determination of phase equilibria in the Co-Cr-Ni system. *J. Phase Equilibria. Diffus.* **35**, 178–185 (2014).
32. Tanaka, K. & Inui, H. Microstructural change of monocrystalline Co-Al-W-based γ/γ′ two phase alloys by high temperature creep. *The 8th Pacific Rim International Congress on Advanced Materials and Processing*, 409–414 (Springer, 2013).
33. Xue, F., Wang, M. & Feng, Q. Alloying effects on heat-treated microstructure in Co-Al-W-base superalloys at 1300 °C and 900 °C. *Superalloys* **2012**, 813–821 (2012).
34. Xue, F. et al. Effects of Ni on microstructural evolution and γ′ dissolution of novel Co-Al-W base alloys. *Acta Metall. Sin.* **50**, 845–853 (2014).
35. Xue, F., Zhou, H. J. & Feng, Q. Improved high-temperature microstructural stability and creep property of novel Co-base single-crystal alloys containing Ta and Ti. *JOM* **66**, 2486–2494 (2014).
36. Yan, H. Y. et al. Alloying and the micromechanics of Co–Al–W–X quaternary alloys. *Mater. Sci. Eng. A.* **613**, 201–208 (2014).
37. Pyczak, F. et al. The effect of tungsten content on the properties of $L1_2$-hardened Co–Al–W alloys. *J. Alloy. Compd.* **632**, 110–115 (2015).
38. Titus, M. S. High temperature deformation mechanisms of $L1_2$-containing Co-based superalloys (University of California Santa Barbara, 2015).
39. Titus, M. S., Eggeler, Y. M., Suzuki, A. & Pollock, T. M. Creep-induced planar defects in $L1_2$-containing Co- and CoNi-base single-crystal superalloys. *Acta Mater.* **82**, 530–539 (2015).
40. Christofidou, K. A. et al. The microstructure and hardness of Ni-Co-Al-Ti-Cr quinary alloys. *J. Alloy. Compd.* **688**, 542–552 (2016).
41. Yan, H. Y. et al. Quaternary alloying effects and the prospects for a new generation of Co-base superalloys. *Superalloys* **2012**, 705–714 (2012).
42. Yan, H. Y., Vorontsov, V. A. & Dye, D. Alloying effects in polycrystalline γ′ strengthened Co–Al–W base alloys. *Intermetallics* **48**, 44–53 (2014).
43. Makineni, S. K., Nithin, B. & Chattopadhyay, K. Synthesis of a new tungsten-free γ–γ′ cobalt-based superalloy by tuning alloying additions. *Acta Mater.* **85**, 85–94 (2015).
44. Bauer, A., Neumeier, S., Pyczak, F., Singer, R. F. & Göken, M. Creep properties of different γ′-strengthened Co-base superalloys. *Mater. Sci. Eng. A.* **550**, 333–341 (2012).
45. Shi, L., Yu, J. J., Cui, C. Y. & Sun, X. F. Effect of Ta additions on microstructure and mechanical properties of a single-crystal Co–Al–W-base alloy. *Mater. Lett.* **149**, 58–61 (2015).
46. Shi, L., Yu, J. J., Cui, C. Y. & Sun, X. F. Temperature dependence of deformation behavior in a Co–Al–W-base single crystal superalloy. *Mater. Sci. Eng. A.* **620**, 36–43 (2015).
47. Shi, L., Yu, J. J., Cui, C. Y. & Sun, X. F. Microstructural stability and tensile properties of a Ti-containing single-crystal Co–Ni–Al–W-base alloy. *Mater. Sci. Eng. A.* **646**, 45–51 (2015).
48. Dunand, D. et al. Designing nanoscale precipitates in novel Cobalt-based superalloys to improve creep resistance and operating temperature (Northwestern University, 2016).
49. Zenk, C. H. et al. A novel type of Co–Ti–Cr-base γ/γ′ superalloys with low mass density. *Acta Mater.* **135**, 244–251 (2017).
50. Bauer, A., Neumeier, S., Pyczak, F. & Göken, M. Microstructure and creep strength of different γ/γ′-strengthened Co-base superalloy variants. *Scr. Mater.* **63**, 1197–1200 (2010).
51. Lass, E. A., Grist, R. D. & Williams, M. E. Phase equilibria and microstructural evolution in ternary Co-Al-W between 750 and 1100 °C. *J. Phase Equilibria. Diffus.* **37**, 387–401 (2016).
52. Lass, E. A., Williams, M. E., Campbell, C. E., Moon, K.-W. & Kattner, U. R. γ′ phase stability and phase equilibrium in ternary Co-Al-W at 900°C. *J. Phase Equilibria. Diffus.* **35**, 711–723 (2014).
53. Zhou, H. et al. Alloying effects on microstructural stability and γ′ phase nanohardness in Co-Al-W-Ta-Ti-base superalloys. *Superalloys* **2016**, 981–990 (2016).
54. Zenk, C. H. et al. Microstructure, lattice misfit, and high-temperature strength of γ′-strengthened Co-Al-W-Ge model superalloys. *Metall. Mater. Trans. A.* **47**, 2141–2149 (2016).
55. Jones, D. R., Schonlau, M. & Welch, W. J. Efficient global optimization of expensive black-box functions. *J. Glob. Optim.* **13**, 455–492 (1998).
56. Caron, P. High γ′ solvus new generation nickel-based superalloys for single crystal turbine blade applications. *Superalloys* **2000**, 737–746 (2000).
57. Stewart, C. A., Murray, S. P., Suzuki, A., Pollock, T. M. & Levi, C. G. Accelerated discovery of oxidation resistant CoNi-base γ/γ′ alloys with high $L1_2$ solvus and low density. *Mater. Des.* **189**, 108445 (2020).
58. Wunderlich, R. K., Fecht, H. J. & Lohöfer, G. Surface tension and viscosity of the Ni-based superalloys LEK94 and CMSX-10 measured by the oscillating drop method on board a parabolic flight. *Met. Mater. Trans. B* **48**, 237–246 (2017).
59. Roebuck, B., Cox, D. & Reed, R. The temperature dependence of γ′ volume fraction in a Ni-based single crystal superalloy from resistivity measurements. *Scr. Mater.* **44**, 917–921 (2001).
60. Akhtar, A., Hook, M. S. & Reed, R. C. On the oxidation of the third-generation single-crystal superalloy CMSX-10. *Metall. Mater. Trans. A.* **36**, 3001–3017 (2005).
61. Pandey, P. et al. Elemental site occupancy in the $L1_2$ A_3B ordered intermetallic phase in Co-based superalloys and its influence on the microstructure. *Acta Mater.* **163**, 140–153 (2019).
62. Pandey, P. et al. On the effect of Re addition on microstructural evolution of a CoNi-based superalloy. *Acta Mater.* **168**, 37–51 (2019).
63. Li, W., Li, L., Antonov, S., Lu, F. & Feng, Q. Effects of Cr and Al/W ratio on the microstructural stability, oxidation property and γ′ phase nano-hardness of multi-component Co–Ni-base superalloys. *J. Alloy. Compd.* **826**, 154182 (2020).
64. Antonov, S. et al. Atom probe tomography investigation on the effect of Ni additions on the site occupation and partitioning behavior in Co-based superalloys. *Microsc. Microanalysis* **25**, 2546–2547 (2019).

ACKNOWLEDGEMENTS

We gratefully acknowledge the financial support of National Key Research and Development Program of China (2016YFB0700505 and 2017YFB0702902), Guangdong Province Key Area R&D Program (2019B010940001) and Scientific and Technological Innovation Foundation of Shunde Graduate School, USTB (BK19BE030). We would like to thank Prof. Yuan Wu and Huihui Zhu for their help on APT characterization. We are grateful to Prof. Ryosuke Kainuma for helpful discussions.

AUTHOR CONTRIBUTIONS

The study was planned and designed by Y.J. and Q.F., machine-learning programs and experiments were performed by P.L., the manuscript prepared by P.L., Y.J., H.Y., and S.A. The STEM characterization was implemented by H.W. All authors discussed the results and commented on the manuscript.

COMPETING INTERESTS

The authors declare no competing interests.

ADDITIONAL INFORMATION

Supplementary information is available for this paper at https://doi.org/10.1038/s41524-020-0334-5.

Correspondence and requests for materials should be addressed to H.H. or Y.S.